

Copyright 2021, ICC & ABRACO

The work presented during 21st INTERNATIONAL CORROSION CONGRESS & 8th INTERNATIONAL CORROSION MEETING in the month of July of 2021.

The information and opinions contained in this work are of the exclusive right of the author(s).

Poster Oral

A decisão final será do Comitê Técnico.

Characterization of the corrosion behavior of sintered parts obtained by powder metallurgy with different manganese sulfide concentrations

Camila B. Nascimento^a, Bruno S. Calabraro^b, Danilo F. Dos Anjos^b, Rafael Evangelista^b,
Sabrina S. Pirielli^b, Marco A. Colosio^c, Jesualdo Luiz Rossi^d

Abstract

Powder metallurgy is a process widely used in automotive parts, such as gears and pistons. The presence of pores is an inherent characteristic of this process. This porosity directly affects machinability, thus making the surface finish of the material rough. One of the alternatives for improving machining is the addition of manganese sulfide (MnS) to the mix composition. This work aimed to investigate the corrosion behavior of an automotive part with a majority iron composition obtained by powder metallurgy with different concentrations of 0%, 0.5% and 1.0% MnS (mass %) and varied densities (5800 kg.m⁻³, 6200 kg.m⁻³ and 6600 kg.m⁻³) in immersion times of 1 h, 4 h, 8 h and 24 h in 3.5% NaCl solution (mass %). The work was undertaken by means of electrochemical tests (electrochemical impedance spectroscopy and potentiodynamic polarization) and microstructural characterization, before and after the immersion periods. The results obtained by electrochemical impedance spectroscopy revealed a drop in the corrosion resistance of the samples as the period of immersion in the electrolyte increased, where the condition without the presence of MnS showed higher corrosion resistance than the samples without MnS. The potentiodynamic polarization curves indicated a reduction in corrosion resistance with an increase in the percentage of MnS in the mixture composition.

Keywords: powder metallurgy, manganese sulfide, corrosion of sintered material

* * *

1 Introduction

The idea of powder metallurgy is quite old one, with artifacts from this technique, such as spears and utensils, dated from 3000 BC, obtained by the union of metallic particles and sintered by hammering (CHIAVERINI, 2001). However, for industry, the technique can be considered recent (from the 19th century), when compared to other older metallurgical processes such as smelting. Corrosion can be defined as the deterioration of a material due to the action of the chemical or electrochemical environment, which may or may not be combined with mechanical stress. This deterioration is caused by the physical-chemical interaction between the material and its operational environment. In metallic parts manufactured using powder metallurgy, this chemical attack occurs not only on the surface of the material, but can also be initiated within the part (MCCAFERTY, 2010). The industry is always looking for ways to develop processes and methods with the purpose of improving the corrosion resistance of manufactured parts

^a Master, Materials Engineer - Centro Universitário Fundação Santo André - FSA

^b Materials Engineer - Centro Universitário Fundação Santo André - FSA

^c Dr., Materials Engineer - General Motors América do Sul - GM

^d Dr., Materials Engineer - Instituto de pesquisas Energéticas e Nucleares - IPEN

using the powder metallurgy technique, since this is a recurring problem and with that many methods have been developed for this impact to be reduced.

Manganese sulfide, in powder metallurgy, started to be used in the last century for the purpose of lubrication. Regarding shock absorber, the piston holes must be machined for the oil to pass through the chambers. This machining process is facilitated so that the breaking of the chips occurs more easily, in addition to increasing the durability of the tooling (KULKARNI et al, 2018). However, according to studies, despite of the benefits mentioned, manganese sulfide decreases the corrosion resistance of the product due to its hygroscopic properties that absorbs moisture (HU et al., 2008). In the present work, the influence of the percentage of MnS, as well as different part densities, on the corrosion resistance of an automotive part produced by powder metallurgy, was analyzed, in order to suggest an alternative to improve properties and corrosion behavior. The project is also a contribution to the bibliography, since very few publications, and not fully related with the subject, were come across during the work.

2 Objective

This work was aimed to investigate the corrosion behavior of an automotive part, shock absorber piston, with a major composition of iron obtained using powder metallurgy with different concentrations of MnS (0%, 0.5% and 1.0 %) and varying densities (5800 kg.m⁻³, 6200 kg.m⁻³ and 6600 kg.m⁻³) in immersion times of 1 h, 4 h, 8 h and 24 h in a 3.5% NaCl solution (mass %). The analyzes were performed through electrochemical tests using electrochemical impedance spectroscopy and potentiodynamic polarization, following the microstructural characterizations, before and after the immersion periods, performed using metallographic and stereoscopic analysis.

3 Experimental

3.1 Materials and test specimens

The samples were obtained based on the Metals Powder Federation Industry standard MPFI 35, mixture F-0005 iron and carbon steel and its compositions were presented in Table 1 (MPIF, 2020).

Table 1 - Components percentage presented in the mixtures A, B and C (mass %).

Compounds	Mixture A	Mixture B	Mixture C
Reduced iron powder	63.2	62.7	62.2
Atomized iron powder	36.0	36.0	36.0
Graphite	0.5	0.5	0.5
Wax	0.3	0.3	0.3
MnS	0	0.5	1.0

The powder amount of all components was adjusted varying the manganese sulfide amount (Table 2). The mixtures were weighed for specimen's compaction in a universal testing machine. The specimens for each mixture (variation of MnS) were obtained, allowing conditions for each variation mixture: A1, A2 and A3, B1, B2 and B3 and C1, C2 and C3. The number 1 is related to the density of 5800 kg.m⁻³, number 2 to 5800 kg.m⁻³, and 3, to 6600 kg.m⁻³. It has been prepared 27 samples.

Table 2 - Elements components (g) presented in the mixtures A, B and C by MPFI standard 35 (MPIF, 2020).

Compounds	Mixture A	Mixture B	Mixture C
Reduced iron powder	175.9	174.5	173.1
Atomized iron powder	100.2	100.2	100.2
Graphite	1.4	1.4	1.4
Wax	0.8	0.8	0.8
MnS	0	1.4	2.8

After compaction, the samples were sintered for 105 minutes at 1100 °C. Then, the specimens were cut into small cylindrical pieces for subsequent characterization. The specimens were in the form of round discs with a diameter of 24.89 mm and a height of 10.16 mm. Three specimens were prepared for each condition and were ground up to grit P2000 using silicon carbide waterproof papers followed by polishing with diamond paste 6 µm.

3.2 Characterization

The surface morphology of the specimens was examined using an optical microscopy. The samples were cut in the cut off machine, hot embedded with Bakelite and sanded with granulation from # 600 to # 1200 as well as being attacked with Nital 2% (nitric acid and alcohol volume %), washed with distilled water and air dried. The Brinell hardness test was performed at three different points of the samples to calculate averages.

EIS measurements were performed using a potentiostat / galvanostat. A conventional three-electrode cell configuration was employed with a platinum wire as the auxiliary electrode, Ag|AgCl as the reference electrode and the mixtures A, B and C specimens as the working electrode. The tests were conducted in a 3.5 % NaCl (mass %) solution at room temperature. Initially, the open circuit potential (*OCP*) was monitored for 1 h. Next, EIS plots were acquired at the *OCP* with a sinusoidal perturbation of ±10 mV (rms) in the frequency range of 100 kHz to 1 Hz at an acquisition rate of 10 points per decade. Different immersion times were assessed; 1 h, 4 h, 8 h and 24 h. Potentiodynamic polarization tests were conducted right after the EIS measurements by sweeping the potential from -300 mV versus the *OCP* up to +1.0 V (Ag|AgCl) at a scan rate of 1mV.s⁻¹.

4 Results and discussion

4.1 Microstructure characterization

The metallographic analyzes present different regions, where, according to the literature, the lighter region is related to the predominant composition of iron, the dark regions, to the pores, and the ashes can be related to the presence of manganese sulfide, a compound which is also present in the mixture (KULKARNI et al, 2018). It was also noted that manganese sulfide is preferentially lodged in the vicinity of the pores (WANG, 2002). Such regions can be seen in Figures 1, 2 and 3, which correspond to the samples of mixture A, B and C.

Note that the samples in Figure 1 (without the addition of MnS), the presence of grayish color superimposed on black (pores) is not observed. In the second sequence of images (samples B1, B2 and B3 with 0.5% MnS concentration), it is possible to observe in some porosity the gray color that indicates the presence of manganese sulfide (MnS) in its chemical composition. In samples C1, C2 and C3, which contains an even higher concentration of MnS (1.0%), it is possible to observe a higher amount of MnS in the porosity of the sample. In samples A1, B1 and C1, where the density is lower (5800 kg.m⁻³), the amount of porosity is higher. In samples A2, B2 and C2, with a higher density, the porosity observed in the microscope was intermediate, the density of 6200 kg.m⁻³ being the usual one in the manufacture of the parts with this

composition. Samples A3, B3 and C3, with a higher density, it is possible to observe from the images that the packaging was higher and hence, the lesser porosity.

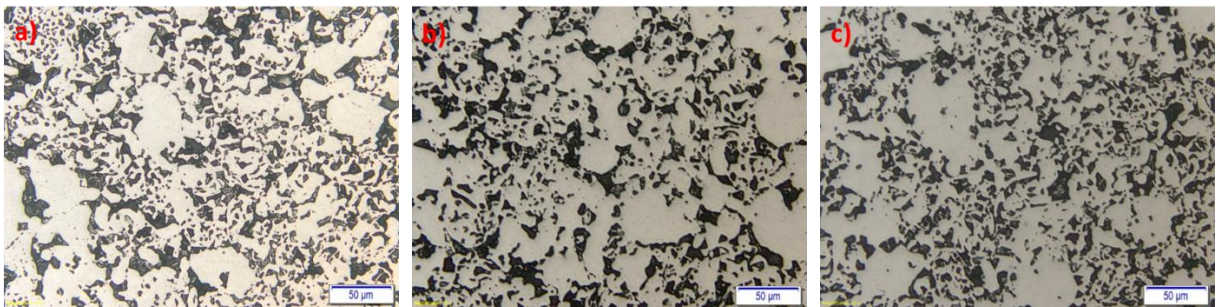


Figure 1 - Micrograph obtained by optical microscopy of mixture A samples a) A1, b) A2 and c) A3.

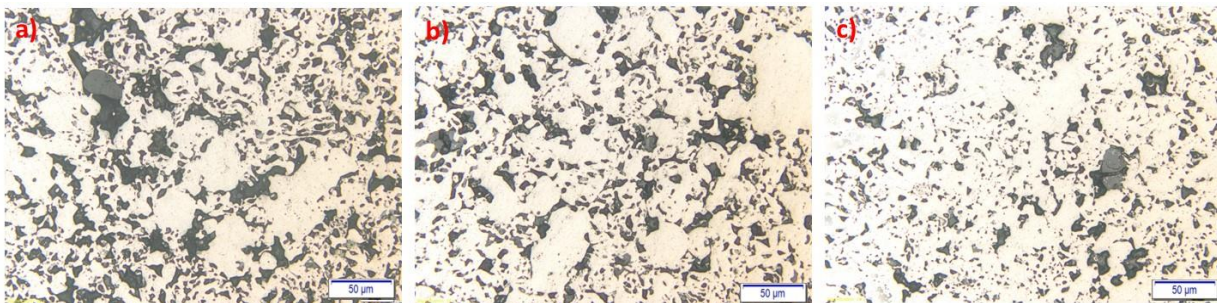


Figure 2 - Micrograph obtained by optical microscopy of mixture B samples: a) B1, b) B2 and c) B3.

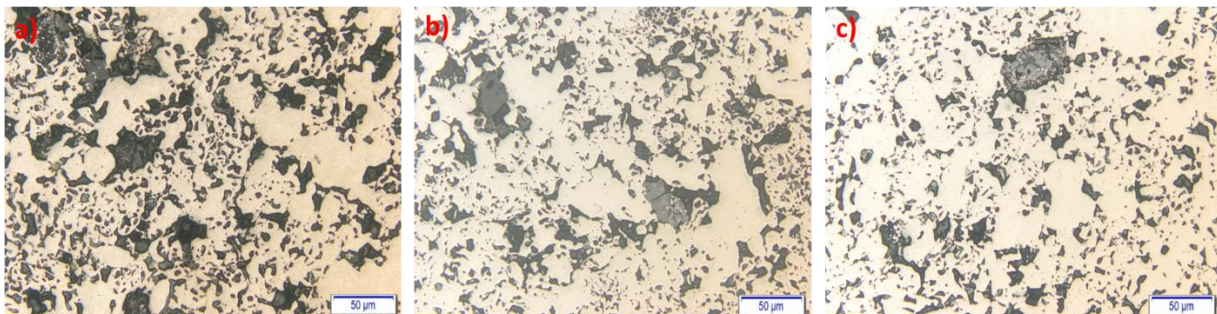


Figure 3 - Micrograph obtained by optical microscopy of mixture C samples: a) C1, b) C2 and c) C3.

4.2 Brinell Hardness

According to results obtained through the Brinell hardness test in which samples of different concentrations of MnS were subjected to three measurements, a tendency was noted that the hardness of the samples was influenced by the density of the conditions. Condition 3 samples (with higher density and less porosity), showed higher hardness values, therefore, they tend to be more fragile, and consequently more susceptible to mechanical failure. Condition 1 of all samples showed a lower hardness due to its lower density, while condition 2 presented an intermediate hardness. The values for the hardness averages found and their standard deviations are shown in Table 3.

Table 3 - Results from the Brinell hardness test for samples A, B and C.

Samples	Average hardness (HB)	Standard deviation
A1	12	2
A2	34	2
A3	56	3
B1	25	2
B2	41	2
B3	45	3
C1	22	3
C2	31	2
C3	44	2

4.3 Electrochemical testing

4.3.1 EIS measurements

Figure 4 shows the Nyquist plots of the A1, A2 and A3 samples after different immersion times in 3.5 % of NaCl (mass %) solution at room temperature. Nyquist diagrams are characterized by a capacitive arc that relates to the corrosion resistance of the material, the greater the radius of the semi-circle of the material, the higher the corrosion resistance (OLIVEIRA, 2014).

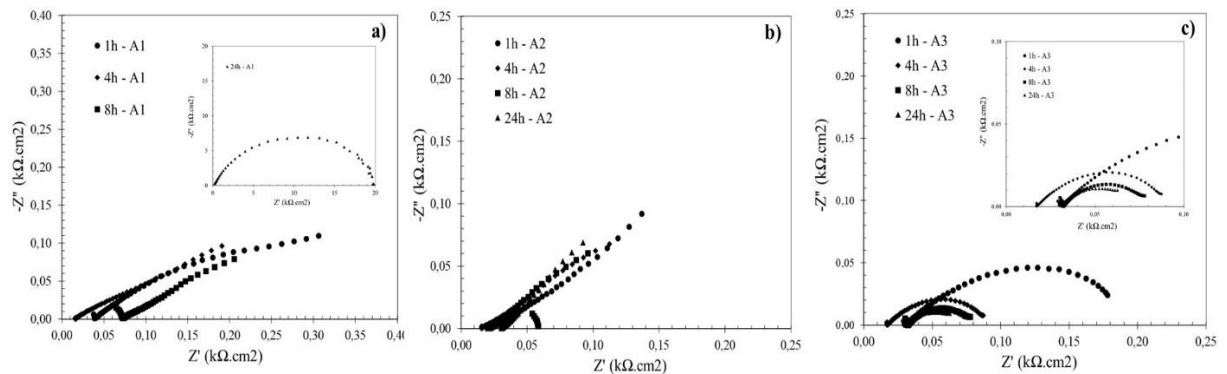


Figure 4 - Nyquist plots of A1, A2 and A3 samples after different immersion times in 3.5% NaCl (mass %) solution at room temperature.

Figure 4.a, presents; the results for sample A1, where the immersion conditions of 1 h and 4 h showed a similar and greater capacitive behavior when compared to the immersion time of 8 h. In the detail of Figure 4.a, the behavior against the corrosion of the sample is presented for the time of 24 h, where it is possible to observe a higher capacitive behavior when compared to the other immersion conditions. For sample A2 (Figure 4.b), a more capacitive behavior can be observed for the sample with immersion time of 1 h and 4 h, followed by times of 8 h and 24 h, which showed similar behaviors. In Figure 4.c, it is possible to observe a marked and well-defined behavior for all immersion periods for sample A3, with a time of 1 h with the highest corrosion resistance and 24 h with the shortest.

Figure 5 details the Bode diagram for phase angle for samples of mixture A, A1, A2 and A3. Corrosion resistance is measured considering the permanence of the curves over long frequency ranges at phase angles closer to -80° and -90° (MCCAFERTY, 2010). In Figure 5.a, the Bode diagram for phase angle for sample A1 is presented, which presents values of phase angles close to the immersion times of 1 h and 4 h at low frequencies, followed by the condition of 8 h. The

immersion time of 24 h presented a phase angle of approximately -60° at frequencies of 3.0 Hz to 5.0 Hz. The same behaviors for all immersion times are observed in the Nyquist diagram. For sample A2 (Figure 5.b), it can be seen that all immersion time conditions behaved similarly and remained so for a long period of frequency, with the phase angle found for the condition of 1 h of approximately -20° (condition which presents higher corrosion resistance) and for the condition of 24 h of immersion a value of approximately -9° (less corrosion resistance). Figure 5.c represents the phase angle Bode diagram for sample A3. The behavior under the conditions of 1 h and 4 h is similar throughout the frequency range, with the largest phase angle at approximately -28° . The 8 h condition showed an intermediate capacitive behavior, remaining at an angle of approximately -8° for a frequency range of 1.5 Hz to 5.0 Hz. For the 24 h immersion time, as pointed out in the Nyquist diagram, the phase angle shown by the Bode diagram showed less corrosion resistance.

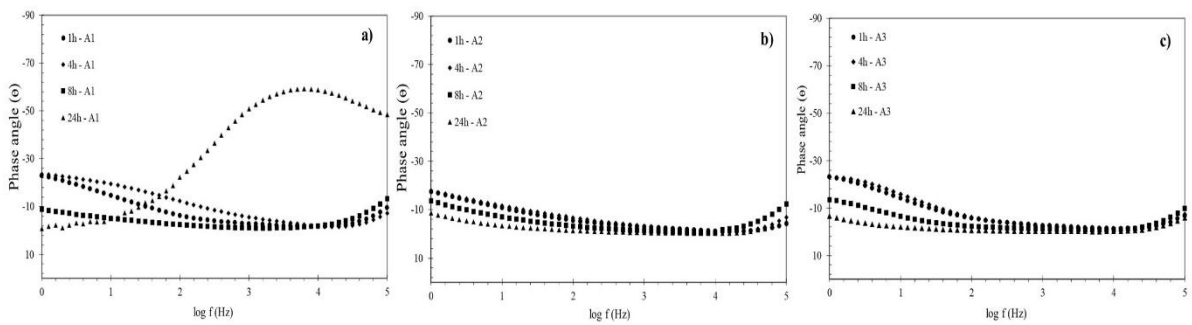


Figure 5 - Bode plots (phase angle) of A1, A2 and A3 samples after different immersion times in 3.5% NaCl (mass %) solution at room temperature.

Figure 6 shows the Nyquist diagram of mixture B for samples B1, B2 and B3. The corrosion behavior for sample B1 is shown in Figure 6.a, where a larger capacitive arc can be seen for the 1 h immersion condition, followed by the 4 h and 8 h. The 24 h immersion condition presented a behavior similar to that observed for the 8 h immersion condition, as shown in the detail of the same figure. For sample B2 (Figure 6.b), it is observed that the samples showed decreasing capacitive behaviors when increasing the immersion time, as shown in the detail of the figure. Figure 6.c shows the Nyquist diagram for sample B3, where it is possible to notice a higher capacitive behavior for the immersion time of 1 h, followed by 4 h, 8 h and 24 h. In detail, it is possible to observe the behavior for the immersion time of 24 h which has a capacitive arc with a smaller diameter and a low impedance value.

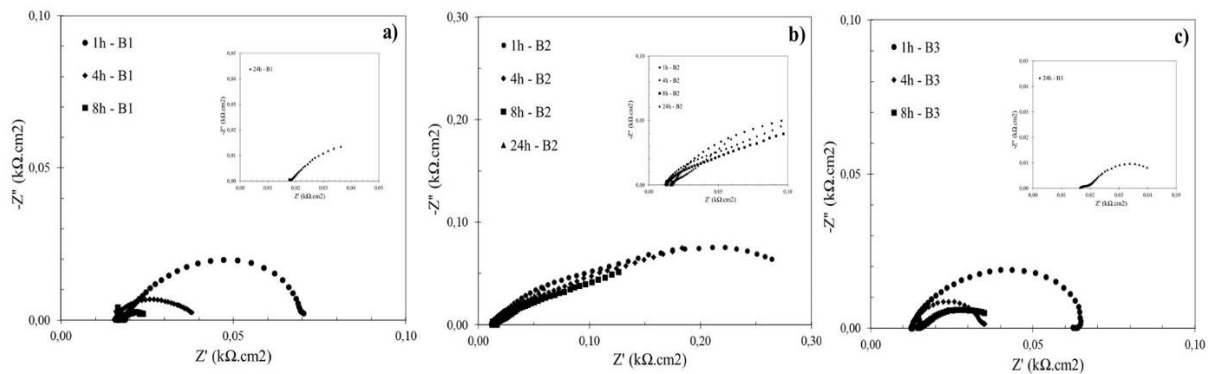


Figure 6 - Nyquist plots of B1, B2 and B3 samples after different immersion times in 3.5% NaCl (mass %) solution at room temperature.

Figure 7 shows the phase angle Bode diagram for samples B1, B2 and B3 of mixture B. For sample B1, phase angle values from -10° to -30° can be noted for the immersion time of 1 h (higher corrosion resistance), already for the immersion time of 4 h, values of phase angle of -5° to -18° are found in a range of low frequencies from 0 Hz to 1.6 Hz. behavior for 8 h and 24 h immersion conditions remain similar also for the Bode diagram.

The Bode diagram for phase angle of sample B2 is shown in Figure 7.b, where it is noted that it remains at an angle of -30° at a frequency range from 0 Hz to 1.0 Hz for the immersion condition of 1 h, with a reduction up to approximately -10° and remaining at this angle until high frequencies. The immersion condition presents a behavior similar to that of 1 h, while for the immersion condition of 8 h it presents a phase angle of approximately -25° at low frequencies, and the immersion condition of 24 h, angles that vary from -5° to -11° , presenting less corrosion resistance.

The results obtained for sample B3 are shown in Figure 7.c, where it is possible to notice a maximum phase angle of approximately -30° at low frequencies for the immersion time of 1 h, remaining at an angle of approximately -8° de 2.0 Hz to 4.5 Hz. For the sample with immersion time of 4 h, phase angles between -8° to -20° can be observed at low frequencies, remaining at -8° at approximately 1.6 Hz to 4.5 Hz. The phase angle for the 24 h condition presented values that oscillate between -8° and -10° . Such behaviors seen in the Bode diagrams can be related to those obtained in the Nyquist diagrams.

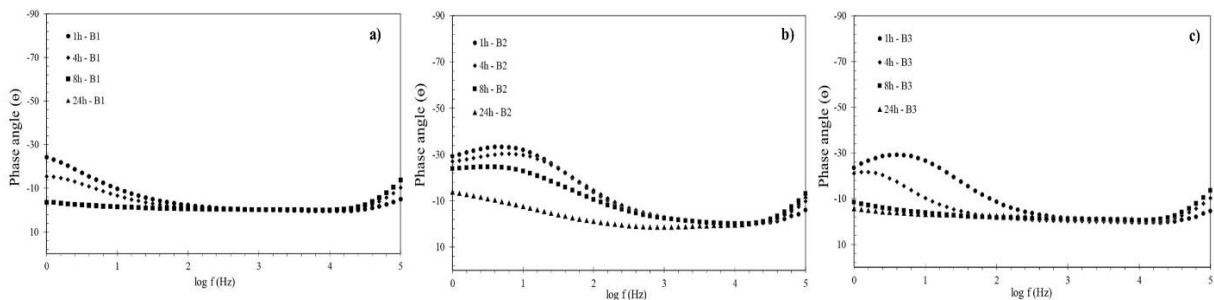


Figure 7 – Bode plots (phase angle) of B1, B2 and B3 samples after different immersion times in 3.5% NaCl (mass %) solution at room temperature.

The Nyquist diagrams of samples C1, C2 and C3 of mixture C are seen in Figure 8. For sample C1 (Figure 8.a), a capacitive arc with a larger diameter is observed, indicating a more capacitive behavior when compared to other conditions of immersion of 4 h, 8 h and 24 h. Figure 8.b represents the Nyquist diagram for sample C2, where for the immersion condition of 1 h, a capacitive arc with a larger diameter is observed, followed by the immersion condition of 4 h. The immersion conditions of 8 h and 24 h showed similar behaviors. The C3 sample has its corrosion behavior represented by the Nyquist diagram in Figure 8.c, where the behavior is striking for each immersion condition. The immersion condition of 1 h showed the highest capacitive arc, followed by the condition of 4 h, 8 h and 24 h.

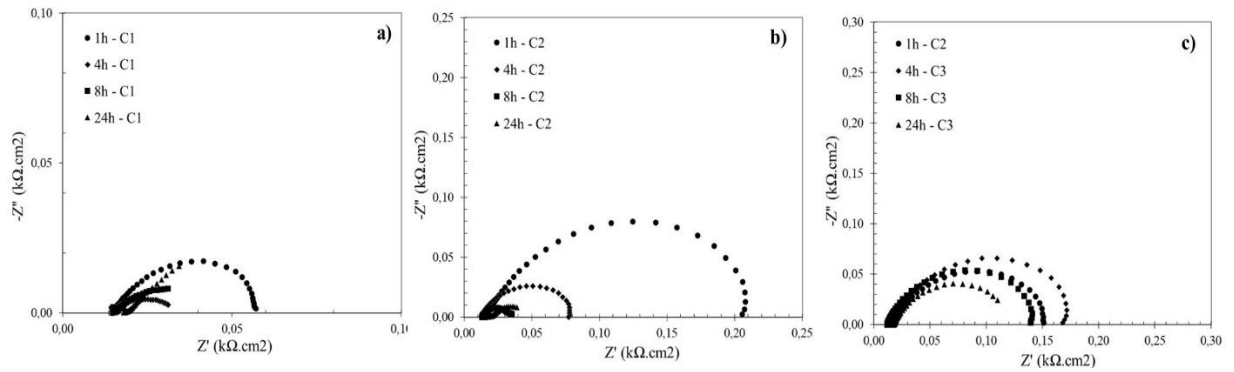


Figure 8 – Nyquist plots of C1, C2 and C3 samples after different immersion times in 3.5% NaCl (mass %) solution at room temperature.

Figure 9 shows the results of the Bode diagram of mixture C for samples C1, C2 and C3. Figure 9.a presents the results obtained for the sample C1, where an angle of -9° to -28° is reached in a frequency range of 0 Hz to 2.0 Hz. The immersion condition of 4 h presented an angle just above of those found for the 8 h and 24 h conditions, exhibiting a behavior similar to them at frequencies from 1.8 Hz to 4.5 Hz. For sample C2 (Figure 9.b), it can be noted a more capacitive behavior for the immersion condition of 1 h, where an angle of approximately -48° is reached at low frequencies, with a reduction starting at 1.0 Hz. The condition of 4 h of immersion presented a maximum angle of -32° , reducing from medium frequencies, and this behavior was also observed for the 8 h condition. For the 24 h immersion condition, an angle of approximately -8° can be observed. Figure 9.c, referring to sample C3, shows a higher corrosion resistance in 4 h and 8 h, reaching an angle of approximately -44° at lower frequencies. The 1 h condition showed results similar to those of 4 h and 8 h, but its angle reached about -40° at low frequencies, until it stabilized at -5° , at the frequency of 2.0 Hz. The smallest capacitive arc was that of the condition 24 h, reaching about -8° at low frequencies and stabilizing with the others at -5° at a frequency of 2.0 Hz.

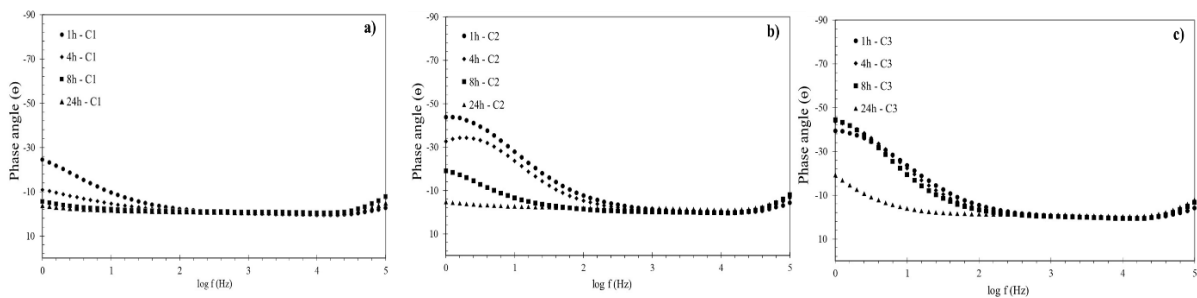


Figure 9 – Bode plots (phase angle) of C1, C2 and C3 samples after different immersion times in 3.5% NaCl (mass %) solution at room temperature.

4.3.2 Potentiodynamic polarization

Potentiodynamic polarization curves of samples A2, B2 e C2 are shown in Figure 10. Tests were conducted right after the EIS measurements. These samples were chosen due to its usual density used in industry (6200 kg.m^{-3}). After the analysis of obtained curves, it was possible to calculate the corrosion potential (E_{corr} V Ag|AgCl) and the corrosion current (i_{corr}).

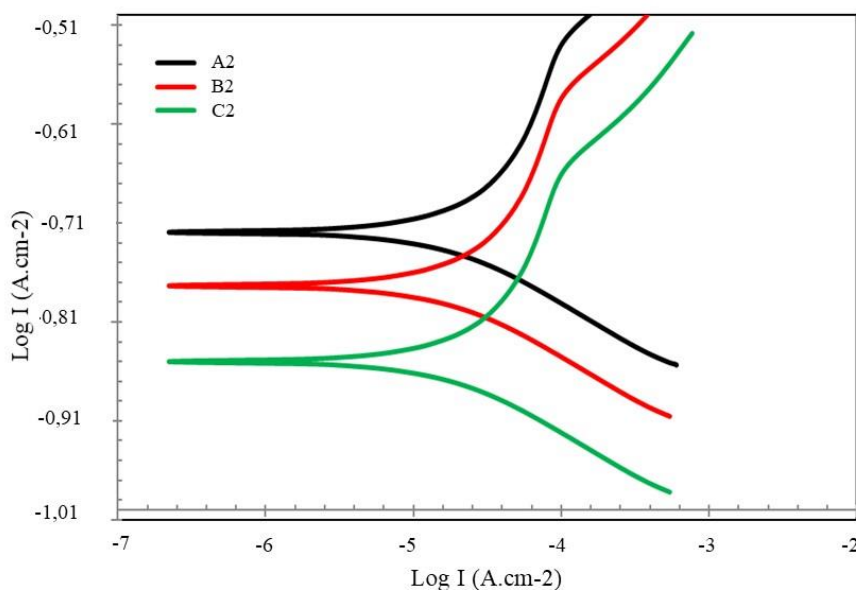


Figure 10 - Potentiodynamic polarization curves of A2, B2 and C2 samples.

For sample A2, the corrosion potential found showed a value of -0.71 V with corrosion current with a value of $7.94 \mu\text{A}\cdot\text{cm}^{-2}$. For sample B2, the value of the corrosion potential was -0.77 V and the corrosion current was $8.31 \times 10^{-5} \text{ A}\cdot\text{cm}^{-2}$. Sample C2 showed a corrosion potential of -0.85 V with a corrosion current value of $8.91 \times 10^{-5} \text{ A}\cdot\text{cm}^{-2}$. The corrosion potential for sample A2 (-0.71 V) was shifted to more noble values compared to the potentials presented for the other conditions, also showing a lower corrosion current value, $7.94 \mu\text{A}\cdot\text{cm}^{-2}$ among the conditions. Such values can be explained due to the absence of MnS in its composition. Samples B2 and C2 showed a more anodic corrosion potential, that is, less noble, with values of -0.77 V and -0.85 V, respectively. This difference in values can be related to the presence of MnS in the mixtures' compositions, being 0.5% for mixture B and 1.0% for mixture C (mass %). The values of corrosion current are also in agreement with that found for the corrosion potentials, showing values of $8.31 \mu\text{A}\cdot\text{cm}^{-2}$ and $8.91 \mu\text{A}\cdot\text{cm}^{-2}$ for samples B2 and C2, respectively. From the observation of the three polarization curves, the pitting corrosion activity was not noticed (MCCAFERTY, 2010).

5 Conclusion

From the metallographic analysis, it was observed that the MnS is located, predominantly, close to the pores of the material, which directly influence the corrosion resistance of the material. In the measurement and analysis of hardness, it can be observed that the density had an influence on the results, where the higher the density of the compacted, the greater its hardness, a factor that can be associated with the fragility caused by the porosity.

Regarding the electrochemical tests, it was possible to observe, in general, a low resistance to corrosion, due to the absence of alloying elements in the composition, thus having a lower corrosion resistance. In addition to the presence of porosity that can interfere in this property, which can act as aggressive ion concentrating sites on the surface and inside the part.

According to Nyquist and Bode diagrams, the immersion times directly influenced the corrosion resistance of the samples immersed in a 3.5% NaCl solution, presenting observable results in the mixture C, which has the highest content of MNS (1% mass). The potentiodynamic polarization curves indicated that the corrosion resistance decreased with the increase in the percentage of manganese sulfide in the mixture, since the lowest corrosion potential found was for sample C2, which had 1.0% (mas %) of MnS in its mixture, being the

noblest corrosion potential found for sample A2, which did not present this element in its mixture. Thus, it is possible to conclude that despite the lubricating characteristics present in MnS in powder metallurgy, it can impair the corrosion resistance of the part when its concentrations in the material composition are increased.

Acknowledgment

The author acknowledges the company Magnet-Marelli Brazil for samples compaction and sintering facilities.

References

CHIAVERINI, V. Powder metallurgy: technique and products. ABM - Associação Brasileira de Metalurgia, São Paulo, 2^a ed., 352 p., 2001. (In Portuguese)

GERMAN, R. Sintering: from empirical observations to scientific principles. Butterworth-Heinemann Elsevier, Langford Lane, Kidlington, Oxford, 2nd ed., 535 p., 2014.

HU, B., S. SHAH, S.; FALLEUR, J.; WARZEL, R.; MILLIGAN, D.; HOWE, I.; ANDERSSON, O. Performance characteristics of a newly developed machinability additive for pm applications. Advances in Powder Metallurgy & Particulate Materials - presented at PM2008 World Congress, in Washington, USA, p. 1-12, 2008.

KULKARNI, H., DABHADE, V. Influence of MnS in processing and applications of sintered Fe-Cu-C alloys: an overview. Materials Today: Proceedings, vol. 5, i. 9, p. 17277-17283, 2018.

MCCAFERTY, E. Introduction to corrosion science. New York, Springer-Verlag, 1st ed., 302 p., 2010.

MPIF - METAL POWDER INDUSTRIES FEDERATION. Standard 35, Materials Standards for PM Structural Parts, 2020 edition.

OLIVEIRA, M. E. Corrosion assessment of carbon steel plates with and without organometallic coating, in contact with the gasoline / ethanol and diesel / biodiesel systems. Master dissertation, Federal University of Minas Gerais, Brazil. Available in <<https://repositorio.ufmg.br/handle/1843/BUOS-986HTD>>. Accessed May 21 2020. (In Portuguese)

WANG, W. F. Effect of MnS powder additions on corrosion resistance of sintered 304L stainless steels. Powder Metallurgy, vol. 45, i. 1, p. 48-52, 2002.